JOURNAL OF SOLID STATE CHEMISTRY 43, 33–44 (1982)

High-Resolution Electron Microscopy of Microsyntactic Intergrowth in V_nO_{2n-1}

Y. HIROTSU,* Y. TSUNASHIMA, AND S. NAGAKURA

Department of Metallurgy, Tokyo Institute of Technology, Oh-okayama, Meguro-ku, Tokyo, Japan

AND H. KUWAMOTO† AND H. SATO

School of Materials Engineering, Purdue University, West Lafayette, Indiana 47907

Received December 3, 1981

Structural features of the Magnéli phases V_nO_{2n-1} were studied by means of high-resolution transmission electron microscopy. Microsyntactic intergrowth on a unit cell scale of several phases with neighboring n were frequently observed in arc-melted specimens, and this was ascribed to the structural compensation of the local composition fluctuation. Also observed were periodic microsyntaxy, where two neighboring phases intergrow periodically, and the crystallographic shear (*CS*) structure with laterally displaced *CS* planes. The origin of this microsyntactic intergrowth is discussed from the standpoint of the *CS* plane interaction.

Introduction

Among many transition metal oxides, a series of homologous long-period compounds is often observed between two stoichiometric phases with different compositions. Most of them take a layered-type structure or the crystallographic shear (*CS*) structure. They have the following characteristics: (1) They have the same structural symmetry and are constructed from the same structural building units forming one- or two-dimensional long-period structures. (2) The energy of the coherent boundary between two neighboring phases is supposed to be negligibly small, when they coexist. (3) The thermodynamic stability is almost equal for the two neighboring phases, especially when the period is long.

Because of the above characteristics, the neighboring line phases can easily intergrow in narrow bands with a crystallographically common axis. Such an intergrowth has been observed by several authors by means of the lattice imaging technique in electron microscopy in hexagonal ferrites (*1*, *2*) and in Magnéli phase compounds V_nO_{2n-1} (*3*–*6*). It was found that the neighboring phases frequently intergrow in narrow bands on a unit cell scale with common basal plane (hexagonal ferrites) or with common *CS* plane (V_nO_{2n-1}). This type of syntactic intergrowth has been termed microsyntactic intergrowth (*7*).

In the present study, detailed high-reso-

* Present address: Technological University of Nagaoka, Nagaoka, Niigata, Japan.

† Present address: Rockwell International Science Center, Thousand Oaks, California 91360.

0022-4596/82/070033-12$02.00/0

lution lattice image observations were made for V_nO_{2n-1} ($n = 6-8$) in order to establish the physical origin of microsyntaxy. Computer simulations of images were also made for the interpretation of image contrast.

Experimental Procedures

A polycrystalline V_nO_{2n-1} specimen was prepared from a mixture of V_2O_3 and V_2O_5 by arc-melting. For the electron microscopic observation, it was ground into small particles. After being dispersed in acetone, the particles were collected on copper-supported holey carbon films. Selected area diffraction patterns showed that the specimen composition was in a range between V_6O_{11} and V_9O_{17}.

Observations were made with an electron microscope of JEM-100C type operated at 100 kV. A high-resolution objective lens with a spherical aberration constant of 0.7 mm and a chromatic aberration constant of 1.05 mm was used.

Very thin crystal flakes which gave (010)* diffraction patterns were selected. In this case, the incident beam direction (along the *b* axis of V_nO_{2n-1}) is parallel to the *CS* plane and the spot density in the (010)* diffraction pattern is the highest among (*hkl*)*[1] patterns. The beam divergence was about 1×10^{-3} rad. The multiple-beam imaging technique (*8*) was applied by the use of an objective lens aperture limiting the scattering angle within 2.1×10^{-2} rad.

Two characteristic types of images related to the *CS* structure were frequently observed with relatively high image contrast. One is composed of closely spaced bright stripes with spacing of about 3 Å which are obliquely intersected by dark lattice fringes having *CS* plane spacings. The other type gives rows of bright spots along the direction parallel to the *CS* planes, and faint spotty or linear images exist between these rows of bright spots. The image of the former type was usually observed under the condition of about 600 Å under-focus, and the latter under about 900 to 1000 Å underfocus. Most of the images were taken under these conditions and the obtained images were compared with computer-simulated images. In the image calculations, atomic positional parameters given by Horiuchi *et al.* (*9*) were used for V_6O_{11} and V_7O_{13}. For V_8O_{15}, the parameters adopted were estimated from V_6O_{11} and V_7O_{13}. The multiple-beam imaging theory (*10, 11*) was applied and the spherical (*12*) and chromatic (*13*) aberrations of the electron optical system were taken into account, as well as the beam divergence (*14*). The thickness for one slice was 3.5 Å ($=b/2$). The absorption correction was made by adding an imaginary term to the projected potential. The number of the interacting beams used was 523, 611, and 693 for V_6O_{11}, V_7O_{13}, and V_8O_{15}, respectively.

[1] (*hkl*)* and [*hkl*]* represent the plane and the direction in the reciprocal lattice, respectively.

Crystal Structures of V_nO_{2n-1}

The structure of V_nO_{2n-1} is well described as a periodic modulation of the rutile-type VO_2 lattice by the *CS* planes. Horiuchi *et al.* (*9*) have recently refined the crystal structures of V_nO_{2n-1} by single crystal X-ray analysis, especially for V_4O_7 to V_7O_{13}. Single-crystal X-ray structural analysis has also be done by Marezio *et al.* for V_4O_7 and V_5O_9 (*15, 16*). These results revealed that the arrangement of VO_6 octahedra is almost identical to the ideal one derived from the parent rutile-type structure by introducing the *CS* planes periodically (*17*), although the VO_6 octahedra at the *CS* plane are distorted considerably.

Figure 1 shows a perspective view of the V_7O_{13} structure (space group $P\bar{1}$) showing the arrangements of VO_6 octahedra. The triclinic axes are drawn after Horiuchi *et al.* (*9*). For V_nO_{2n-1} structures, relations between the basic translation vectors of the

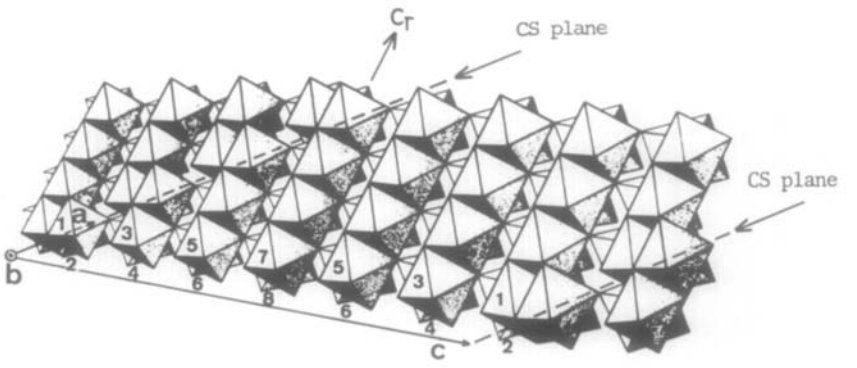

FIG. 1. Perspective view of V_7O_{13}. The triclinic V_7O_{13} structure represented by the arrangement of VO_6 octahedra is viewed along the b axis. The crystallographic shear planes are along the (a,b) plane and the positions are indicated by arrows. Straight chains of the edge-sharing VO_6 octahedra are extending along the c axis of the rutile-type VO_2 structure (along $\mathbf{c}_r$). One unit cell includes 14 VO_6 octahedra, and the numbers 1, 3, 5, and 7 are given to the VO_6 octahedra having the central vanadium atoms at $y = \frac{1}{2}$, and 2, 4, 6, and 8 to those having central vanadium at $y = 0$. The octahedra with even and odd numbers along the b axis share their corners. The dimensional parameters of the unit cell are: $a = 5.439$, $b = 7.005$, and $c = 35.516$ Å. $\alpha = 40.9$, $\beta = 72.6$, and $\gamma = 109.0°$. Space group $P\bar{1}$.

triclinic V_nO_{2n-1} lattice $\mathbf{a}_n$, $\mathbf{b}_n$, $\mathbf{c}_n$ and those of the rutile-type tetragonal VO_2 lattice $\mathbf{a}_r$, $\mathbf{b}_r$, $\mathbf{c}_r$ are $\mathbf{a}_n = -\mathbf{a}_r + \mathbf{c}_r$, $\mathbf{b}_n = \mathbf{a}_r + \mathbf{b}_r + \mathbf{c}_r$, and $\mathbf{c}_n = (2n - 1)(\mathbf{b}_r + \mathbf{c}_r)/2$ (*9*). Therefore, the *CS* plane $(1\bar{2}1)_r$ in the rutile-type lattice corresponds to (001) for the triclinic V_nO_{2n-1} lattice. In the V_7O_{13} structure, the (001) *CS* plane exists at every thirteen oxygen layers parallel to (001). In Fig. 1, the edge- and face-shared VO_6 octahedra are seen in the area of the *CS* plane, while in the slab of VO_2 structure the corner- and edge-shared VO_6 octahedra are seen. The rows of the edge-shared VO_6 octahedra in the VO_2 slab are along the $\mathbf{c}_r$ direction. In the ideal *CS* structure, as drawn in Fig. 1, the *CS* plane can be formed by introducing the $[011]_r/2$ shear to the VO_2 lattice.

The *CS* plane spacing in V_nO_{2n-1}, d_{001}, is shown in Table I in relation to the n value, which is calculated from the crystallographic data (*9, 18*).

TABLE I

INTERPLANER SPACINGS OF *CS* PLANES d_{001}

V_nO_{2n-1}	V_4O_7	V_5O_9	V_6O_{11}	V_7O_{13}	V_8O_{15}	V_9O_{17}
d_{001} (Å)	6.052	7.721	9.386	11.053	12.704	14.365[a]

[a] Extrapolated from the values of V_4O_7 to V_8O_{15}.

Results

a. Microsyntactic Behavior

The intergrown structures composed of V_nO_{2n-1} and its neighboring phase $V_{n'}O_{2n'-1}$ ($n' = n \pm 1$) were often observed to have the common (001) *CS* plane. The width of the neighboring phase was about a few hundred Å. In such a case, the two-component phases gave overlapped diffraction patterns (*3*). However, the growth in the form of microsyntactic intergrowth was observed more frequently. In this case, the diffraction pattern from the matrix phase was accompanied by weak diffuse streaks passing through each diffraction spot in the [001]* reciprocal lattice direction. In most cases, only one neighboring phase was observed. In some cases, however, two neighboring phases were found to intergrow in the matrix; in other words, three phases coexist side by side microsyntactically in some areas. Figure 2a shows a selected area dif-

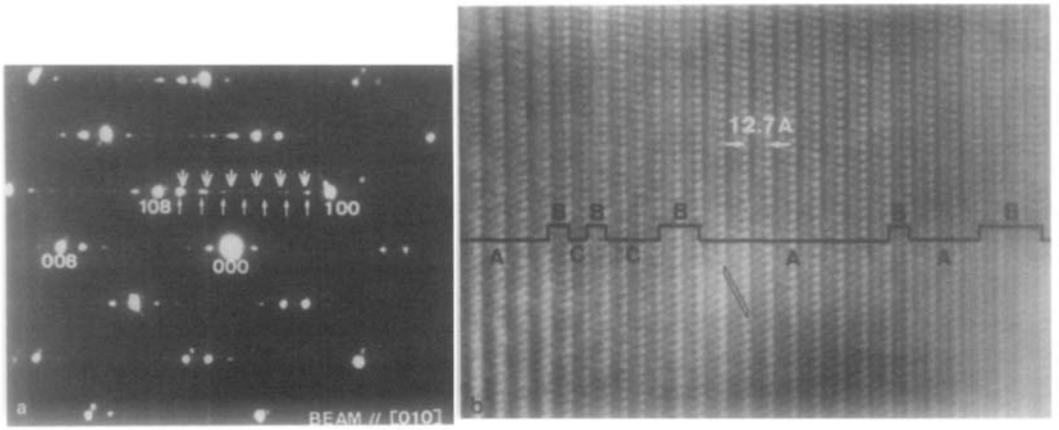

FIG. 2. (a) Selected area diffraction pattern (010)* from an area of microsyntactic intergrowth. A series of diffuse $10l$ spots from intergrown V_7O_{13} structure (down arrows) are seen in the matrix V_8O_{15} diffraction pattern. (b) Multiple-beam lattice image of the area by the use of the diffraction spots shown in (a). Diffracted beams within the scattering angle of 2.1×10^{-2} rad are contributing to the imaging. Rows of bright spots are parallel to the *CS* planes. The regions A, B, and C correspond to V_8O_{15}, V_7O_{13}, and V_6O_{11} structural regions, respectively. The unit cell of V_8O_{15} in A is shown by the parallelogram. The picture was taken under about 1000-Å under-focus condition.

fraction pattern from an area including three such phases. The reflection spots are somewhat diffuse and several extra-reflection spots are seen (downward arrows) besides the series of $10l$ reflection spots from the V_8O_{15} matrix (upward arrows). These extra-reflections were identified to be those from the microsyntactically intergrown V_7O_{13} phase. No other phases can be identified in the diffraction pattern. Figure 2b is the corresponding multiple-beam lattice image. The amount of defocusing was about 1000 Å (under focus). In the image, the rows of bright spots parallel to the (001) *CS* planes are seen, which have three different spacings. The regions having these three different spacings are distinguished in the figure by the letters A, B, and C. It was found that the narrower spacings represented by the letters B and C correspond to those of the (001) *CS* planes of V_7O_{13} and V_6O_{11} structure, respectively. Figures 3a, b, and c are computer-simulated images of V_8O_{15}, V_7O_{13}, and V_6O_{11} structures based on the 1000-Å under-focus condition and the crystal thickness of 70 Å. The arrangements of the rows of bright spots in the simulated images are in good agreement with those in the observed images. In the simulation, the images between the rows of bright spots vary according to the structures, but in the observed images these features are not clear. The image simulation shows that the rows of bright spots are exactly on the line of the projection of the *CS* plane.

From the above results, it can be said that the V_nO_{2n-1} phases are thermodynamically definable down to the unit cell scale width. Since the thermodynamic stabilities of these phases are almost equal (*19*) and the formation energy of the *CS* plane is thought to be smaller to that of the assembly of point defects (oxygen vacancies) for the compensation of the nonstoichiometry (*20*), various phases can coexist especially when the specimens are prepared under nonequilibrium conditions.

b. Periodic Microsyntaxy

In addition to the ordinary microsyntactic intergrowth in which intergrown phase

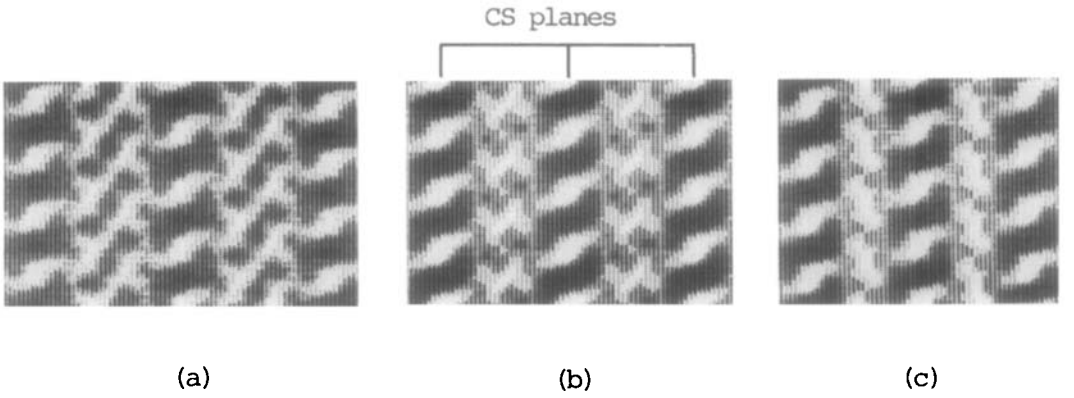

FIG. 3. Calculated images of (a) V_8O_{15}, (b) V_7O_{13}, and (c) V_6O_{11} structure. Amount of defocus $\Delta f =$ 1000 Å. Crystal thickness $D = 70$ Å. The beam incidence direction is inclined from the b axis by an amount of 3×10^{-3} rad to [001]*. The rows of bright spots are on the line of the projections of *CS* planes.

appears in a random fashion, as shown in Fig. 2b, a periodic intergrowth of two neighboring phases is often found. This type of intergrowth was first found in a V_6O_{11} specimen prepared by a vapor transport method and was termed periodic microsyntaxy, where V_6O_{11} and V_7O_{13} intergrew alternatively on a unit cell scale to form $V_{13}O_{24}$ structure (*4*).

Figure 4 shows an example of another

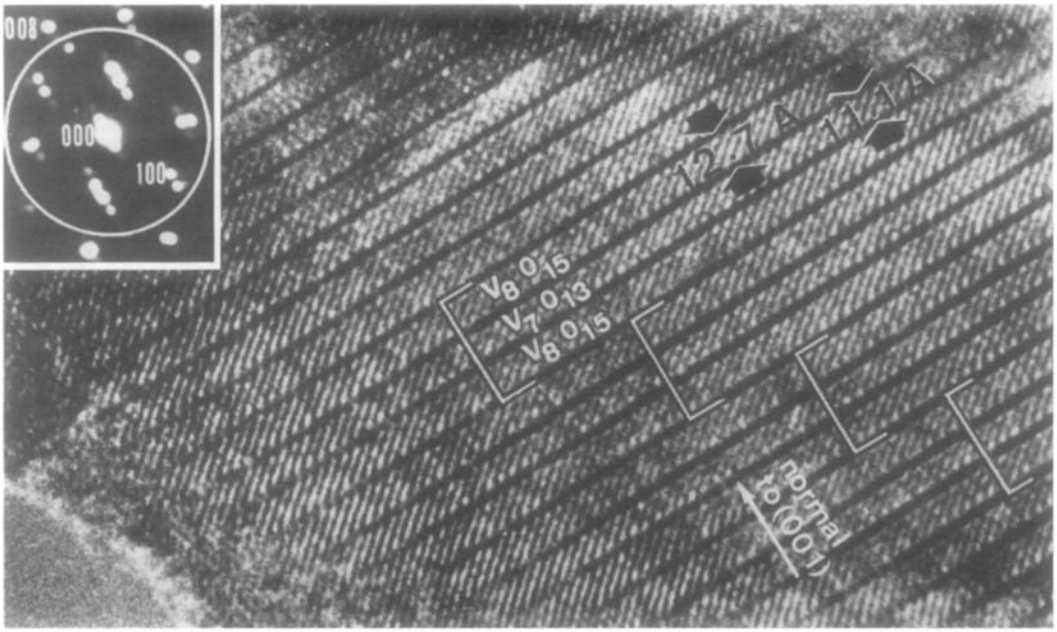

FIG. 4. High-resolution multiple-beam image showing the periodic microsyntactic intergrowth. Beam is incident along the b axis. The image was taken by using the diffraction spots inside the encircled area (scattering angle: 2.1×10^{-2} rad) in the attached diffraction pattern. The focusing condition is about 600 Å under-focus.

type of periodic microsyntaxy found in the present arc-melted specimen. The micrograph was taken under an about 600-Å under-focus condition, which is close to the optimum-focus condition (620 Å underfocus) for the structure image (*8*). In the figure, a periodically modulated structure is seen with boundaries parallel to the (001) *CS* plane in the matrix V_8O_{15}. From the period of the dark lattice fringes parallel to the (001) plane and the fine dark stripes running obliquely to the dark fringes, the unit of the periodically intergrown structure was found to be composed of double V_8O_{15} and single V_7O_{13} unit cells with the common *CS* planes. Therefore, $V_{23}O_{43}$ can be assigned for the periodically intergrown structure.

Since the image was taken under nearly optimum focusing condition, it provides information on the atomic arrangements. Judging from the V_7O_{13} structure shown in Fig. 1, the dark lattice fringes in Fig. 4 may reflect the (001) *CS* planes and the fine dark stripes may also reflect the rows of VO_6 octahedra intersecting the (001) *CS* planes aslant. Structure factor calculations for the *h*0*l* reflections of V_7O_{13} and V_8O_{15} showed that the structure factor coming from vanadium atoms, F^{V}_{h0l}, is always much larger than that from oxygen atoms, F^{O}_{h0l}. The ratio of F^{V}_{h0l}/F^{O}_{h0l} ranges from about 5 to 400 depending on the indices of *h*0*l*. Therefore, the multiple-beam lattice image is mainly contributed by vanadium atoms. Figure 5 shows the atomic arrangement of vanadium atoms in V_7O_{13} viewed along the *b* axis, where they are represented by large (V_{odd}) and small (V_{even}) open circles and their distance is 3.5 Å (=*b*/2) along the *b* axis. These chains of vanadium atoms along the *b* axis are arranged along the $\mathbf{c}'_r$ (= $-6.5\mathbf{a}' + \mathbf{c}'$) direction,[2] which makes an angle of 38°

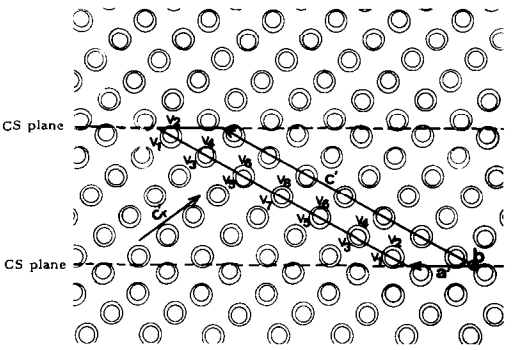

FIG. 5. Atomic arrangements of vanadium atoms in the V_7O_{13} structure viewed along the *b* axis. The atomic rows along the $\mathbf{c}'_r = -6.5\mathbf{a}' + \mathbf{c}'$ direction are shifted at the *CS* plane. The parallelogram indicates the *b* projection of the unit cell. Vanadium atoms indicated by letters V_1, V_3, V_5, and V_7 are separated from those indicated by V_2, V_4, V_6, and V_8 by *b*/2.

to the *CS* plane. The spacing between these vanadium atom rows normal to the $\mathbf{c}'_r$ direction is 3.1 Å. For V_8O_{15}, the structural description is the same if we add another vanadium layer along the (001) *CS* plane and consider the rows of vanadium atoms in the $\mathbf{c}'_r = -7.5\mathbf{a}' + \mathbf{c}'$ direction. Because of the existence of *CS* planes, the rows of vanadium atoms in the $\mathbf{c}'_r$ direction are kinked at the *CS* plane. On the other hand, the observed spacing between the periodically arranged dark fine stripes is about 2.9 Å and the stripes make an angle of about 40° with the dark linear fringes. Thus the observed dark fine stripes may correspond to the rows of vanadium atoms in the $\mathbf{c}'_r$ direction, since according to the electron optical theory of lattice imaging for thin crystal under the optimum-focus condition (*21*), the image intensity is proportional to the projection of the crystal potential. In order to confirm this conclusion, image simulations were made for V_7O_{13} and V_8O_{15} structures under the same imaging conditions as in the experiment. Figures 6a and b show the calculated images corresponding to the crystal thickness of 70 Å. The dark stripes in the simulated images are in good agreement

[2] This corresponds to $\mathbf{c}'_r = -(2n-1)\mathbf{a}'/2 + \mathbf{c}'$, where $\mathbf{a}'$ and $\mathbf{c}'$ are the $\mathbf{a}_n$ and $\mathbf{c}_n$ projected on the plane normal to the *b* axis.

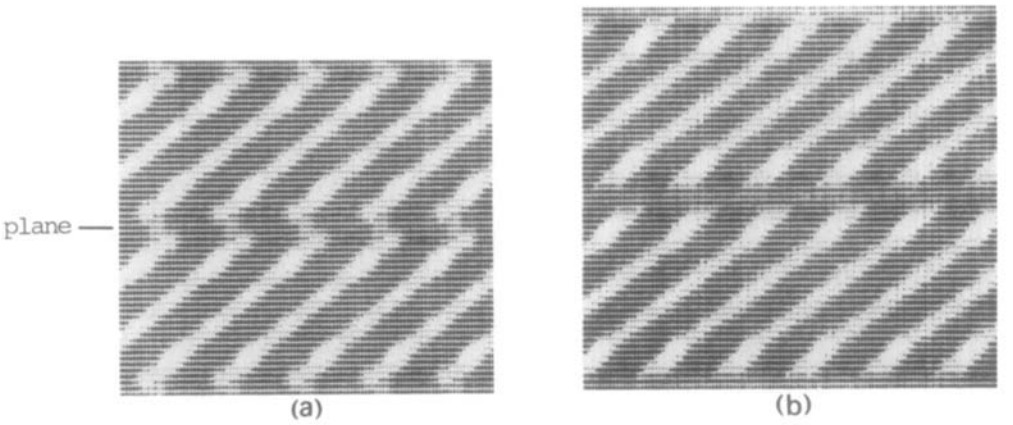

FIG. 6. Calculated images of V_7O_{13} (a) and V_8O_{15} (b). $\Delta f = 600$ Å, $D = 70$ Å. The beam incidence is exactly parallel to the b axis. Bright lines in the calculated image of V_7O_{13} correspond well to the potential valleys of vanadium atoms found in Fig. 5.

with the observed ones with respect to both the spacing and the direction. An examination of the positions of vanadium atoms in the simulated images showed that the bright stripes correspond to the potential valleys between the atomic rows of vanadium. It was also confirmed that the model of $V_{23}O_{43}$ formed by the periodic intergrowth of V_7O_{13} and V_8O_{15} is correct and that the dark lattice fringes intersecting the dark fine stripes really represent the *CS* planes with the spacings of 11.1 Å (V_7O_{13}) and 12.7 Å (V_8O_{15}), respectively.

c. CS Planes with Steps

According to the present lattice image observations of the *CS* structures, most of the images of *CS* planes are straight and parallel to each other. In some cases, however, local variations in the *CS* plane spacings (*CS* planes with steps) have been observed. Figure 7 shows an example of such

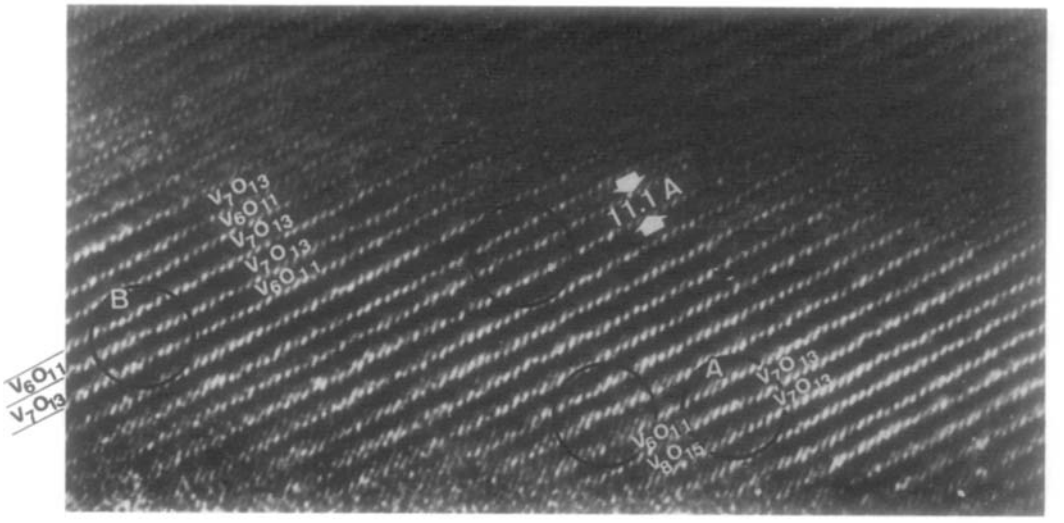

FIG. 7. A multiple-beam lattice image of the structure mainly composed of V_6O_{11} and V_7O_{13}. Steps in the *CS* planes are observed in the encircled areas.

images. The structure is composed of a mixture of V_7O_{13} and V_6O_{11} in most areas. The beam incidence is almost parallel to the common *b* axis and the focusing condition is about 1000 Å under-focus. At several sites, especially in the encircled areas A and B, steps of the *CS* planes are observed. By image simulations of V_6O_{11}, V_7O_{13}, and V_8O_{15} structures, it was confirmed that the observed rows of bright spots are exactly on the lines of the projections of the *CS* planes. By comparing the results of image simulations with the observed images, it was concluded that a pair of V_6O_{11} and V_8O_{15} structural periods changes into the period of V_7O_{13} in the area A, while in B, V_6O_{11} and V_7O_{13} change their arrangements to form a periodic microsyntaxy producing the $V_{13}O_{24}$ structure. Therefore, the step structure in the *CS* plane may represent a transitional stage to a regular *CS* plane formation.

The calculated images of V_6O_{11}, V_7O_{13}, and V_8O_{15} under the same imaging condition are shown in Figs. 8a to c. The projections of the unit cells along the *b* axis are represented by the parallelograms connecting the bright spots *ijkl*. The shape and the dimension of each parallelogram and also the image contrast around the *CS* plane change

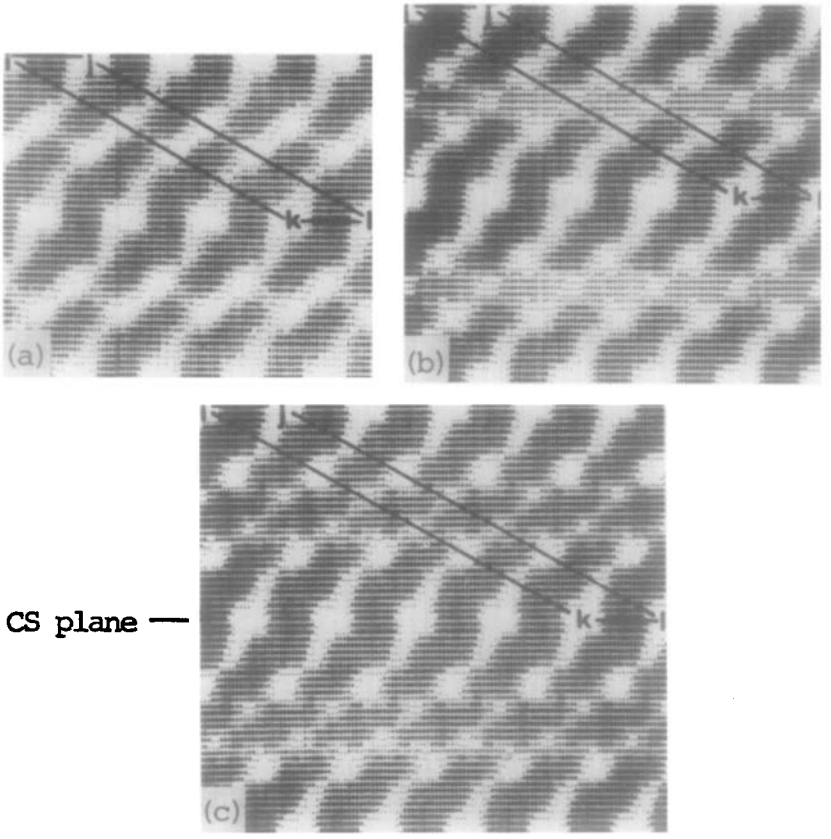

FIG. 8. Calculated images of V_6O_{11} (a), V_7O_{13} (b), and V_8O_{15} (c). Δf = 980 Å, D = 35 Å. The beam incidence is inclined from the *b* axis by 3×10^{-3} rad toward [001]*. In the figures, the rows of bright spots are on the line of the projections of *CS* planes, and the unit cells are shown by the parallelograms connecting *ijkl*.

depending on the structures of V_6O_{11}, V_7O_{13}, and V_8O_{15}.

In arc-melted specimens, which are rather quickly prepared, the thermal history may be different from place to place. Accordingly, it may be possible to observe the intermediate stage of the *CS* plane formation. This possibility will be discussed in the following section.

Discussion

In the arc-melted specimen, the distribution of the microsyntactically intergrown phases is more random than that in specimens grown by the vapor transport technique. The degree of the composition fluctuation is considered to be higher in the arc-melted specimen. Because of the ease of the *CS* plane formation compared with the atomic vacancy formation, the local composition fluctuation is possibly compensated by the microsyntactic intergrowth of the neighboring phases. A high-resolution imaging work seems to be necessary when we examine the solid solubility range of a certain phase which belongs to a series of line phases, because even the selected area diffraction method often fails to detect the existence of the intergrowth of other phases on a unit cell scale as shown in Fig. 2. This kind of argument may become important with respect to the nonstoichiometry in the case of a layered compound like β-alumina (*22–24*).

By electron microscopic studies on the reduction process of TiO_2 (*25, 26*), $(Ti,V)O_2$ (*27*), and MoO_3 (*28*), it has been shown that randomly arranged *CS* planes (Wadsley defects) change into bundles of *CS* planes during the course of reduction, and further into the ordered arrangement of *CS* planes of the Magnéli phase compounds. In order to explain these apparent ordering phenomena of the *CS* planes theoretically, some authors have attempted to estimate the change in the free energy of the crystal by introducing elastic or electrostatic interaction potential between the *CS* planes (*29, 30*). According to their theoretical calculations, the elastic interaction seems to be predominant for the ordered *CS* plane formation. If the reduction of the free energy by the formation of ordered structure is large enough, randomly arranged microsyntactically intergrown structures can change into the ordered structure by further annealing. The periodic microsyntaxy can be a result of such a structural relaxation.

In order to explain the formation of such periodic microsyntactic phases as $V_{13}O_{24}$ and $V_{23}O_{43}$, it may be desirable to introduce the concept of the reduction in the elastic free energy by the formation of periodically arranged microsyntactically intergrown structure. The reduction of the free energy can be understood qualitatively by the following simple argument. In Fig. 9, the average interplanar spacing between the neighboring oxygen layers parallel to the (001) *CS* plane of the V_nO_{2n-1} is plotted against the n value. The crystallographic data by Horiuchi *et al.* (*9, 18*) are used for the calculation. The plot at $n = \infty$ corresponds to the $(1\bar{2}1)$ interplanar spacing of rutile-type VO_2 lattice. The decrease in the average interplanar spacing $d_{001}/(2n-1)$ with n can be interpreted as a result of an elastic repulsive interaction between the *CS* planes. In

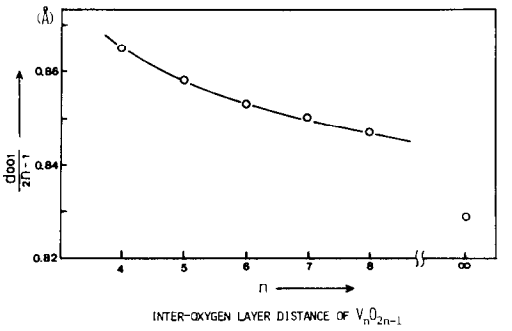

FIG. 9. Dependence of average interoxygen layer distance $d_{001}/(2n-1)$ on n.

this case, for the mixture of V_6O_{11} and V_7O_{13}, for example, a unit structure of V_6O_{11} may exert a compressive stress to the averaged surrounding structure, while a unit structure of V_7O_{13} may exert a tensile stress to it. Therefore, a periodic alternative formation of V_6O_{11} and V_7O_{13} unit structures to form $V_{13}O_{24}$ structure may reduce the strain energy involved in the crystal. This situation is similar to the case of ordered structure formation in a binary alloy whose constituent species are different in atomic size.

It is hard to suppose that a periodic concentration fluctuation on a unit cell scale is first created in the matrix and transforms into the periodic microsyntactic structure. A reasonable formation mechanism of the periodic microsyntactic structure may be that an inhomogeneous *CS* structure is first formed with various *CS* plane spacings from the concentration fluctuation in the specimen and then the *CS* planes rearrange to make the periodic microsyntactic structure. The image in area B in Fig. 7 is considered to show the transitional state toward the formation of the periodic microsyntaxy composed of V_7O_{13} and V_6O_{11}. Similarly, a redistribution process of the *CS* planes to form a homogeneous *CS* structure from an inhomogeneous one, such as $V_6O_{11} + V_8O_{15} \rightarrow 2V_7O_{13}$, may take place in order to reduce the strain energy of the system. The image in area A in Fig. 7 seems to show the transitional state of such a reaction.

Based on the observed *CS* planes with

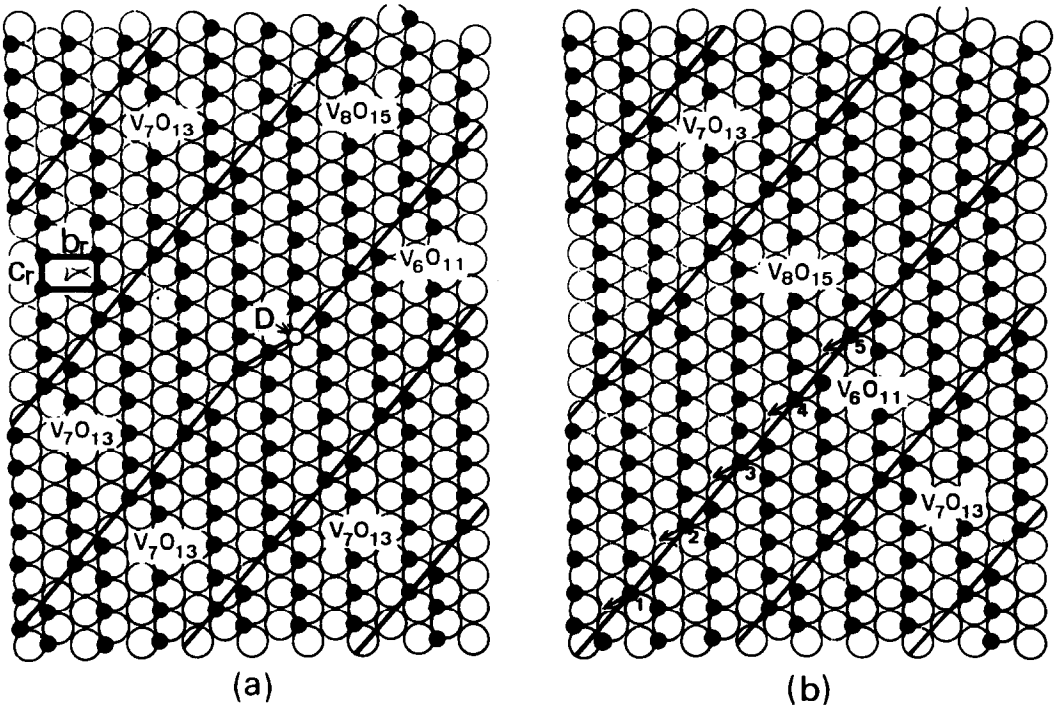

FIG. 10. (a) Atomic arrangement of oxygen (open circle) and vanadium (solid circle) atoms viewed along the *a* axis of the rutile-type VO_2 lattice. This corresponds to the image in area A in Fig. 7, and represents the formation of $2V_7O_{13}$ from V_6O_{11} and V_8O_{15} by the kinking of the *CS* plane. D indicates a vanadium vacancy. (b) A model showing the lateral motion of the *CS* plane to form the structure in (a) by the cooperative jumps of vanadium atoms in the direction indicated by arrows. See that a vanadium vacancy is formed at the step of the *CS* plane.

steps, as shown in Fig. 7, a possible mechanism for the rearrangement of *CS* planes is presented in the following. Figure 10a shows a structural model for the encircled area A in Fig. 7 where V_6O_{11} and V_8O_{15} react to form double V_7O_{13}. The atomic arrangement on an idealized $(100)_r$ plane of the rutile-type VO_2 structure, which corresponds to the $(\bar{1}10)$ plane of V_nO_{2n-1}, is depicted, together with the traces of intersecting *CS* planes (solid lines). The $(1\bar{2}1)_r$ or the (001) V_nO_{2n-1} *CS* plane makes an angle of 110.9° with the $(001)_r$ plane. Oxygen atoms (open circles) are closely packed and vanadium atoms (solid circles) are on them. They make a double atomic layer and stack up in a way so that every double atomic layer is displaced successively by a vector $[110]_r/2$ with respect to the next layer. A vanadium defect site (lettered by D) always exists at the step of the *CS* plane between V_6O_{11} and V_8O_{15}. An energetically most favorable model for the formation of this stepped structure is schematically shown in Fig. 10b, where the movement of vanadium atoms is cooperative along the *CS* plane as indicated by arrows. This model is based on the migration mechanism of *CS* planes proposed by Andersson and Wadsley (*31*). In this model, the step of the *CS* plane can be regarded as a termination point of the cooperative movement of vanadium atoms or as an initiation point of it. In the former sense, the cooperative motion of vanadium atoms must occur one after another, for example, from vanadium 1 to 5 in Fig. 10b, while in the latter sense, the cooperative motion starts from vanadium 5 and propagates to the lower-numbered vanadium atoms. We may call the position at the stepped *CS* plane a nucleation site for the growth process of V_7O_{13} structure, if the position is the initiation site for the cooperative movement of vanadium atoms. The nucleated *CS* structure (V_7O_{13} in this case) can be grown along the direction parallel to the *CS* plane by the cooperative metal atom jumps to give the lateral movement of the *CS* plane. The formation of the periodic microsyntactic structure is also possible by the present model of rearrangement of *CS* planes.

References

1. Y. Hirotsu and H. Sato, *J. Solid State Chem.* **26,** 1 (1978).
2. Y. Hirotsu, H. Sato, Y. C. Tang, and S. Nagakura, "Proceedings of the 3rd International Conference on Ferrites, Kyoto, 1980," p. 345.
3. Y. Hirotsu, S. P. Faile, and H. Sato, *Mater. Res. Bull.* **13,** 895 (1978).
4. Y. Hirotsu and H. Sato, *Mater. Res. Bull.* **15,** 41 (1980).
5. H. Kuwamoto, N. Otsuka, and H. Sato, *J. Solid State Chem.* **36,** 133 (1981).
6. J. R. Gannon and R. J. D. Tilley, *J. Solid State Chem.* **25,** 301 (1978).
7. H. Sato and S. Shinozaki, *Mater. Res. Bull.* **9,** 679 (1974).
8. J. M. Cowley and S. Iijima, *Z. Naturforsch. A* **27,** 445 (1972).
9. H. Horiuchi, N. Morimoto, and M. Tokonami, *J. Solid State Chem.* **17,** 407 (1976).
10. P. Goodman and A. F. Moodie, *Acta Crystallogr. Sect. A* **30,** 280 (1974).
11. J. M. Cowley, "Diffraction Physics," North-Holland, Amsterdam (1975).
12. O. Scherzer, *J. Appl. Phys.* **20,** 20 (1949).
13. P. L. Fejes, *Acta Crystallogr. Sect. A* **33,** 109 (1977).
14. J. Frank, *Optik* **38,** 519 (1973).
15. M. Marezio, D. B. McWhan, P. D. Dernier, and J. P. Remeika, *J. Solid State Chem.* **6,** 213 (1973).
16. M. Marezio, P. D. Dernier, D. B. McWhan, and S. Kachi, *J. Solid State Chem.* **11,** 301 (1974).
17. S. Andersson and L. Jahnberg, *Ark. Kemi* **21,** 412 (1963).
18. H. Horiuchi, M. Tokonami, N. Morimoto, K. Nagasawa, Y. Bando, and T. Takada, *Mater. Res. Bull.* **6,** 833 (1971).
19. J. S. Anderson, "The Chemistry of Extended Defects in Non-Metallic Solids," p. 1, North-Holland, Amsterdam (1970).
20. C. R. A. Catlow, Modulated structures 1979, In "AIP Conference Proceedings No. 53, p. 149 (1979).
21. D. F. Lynch, A. F. Moodie, and M. A. O'Keefe, *Acta Crystallogr. Sect. A* **31,** 300 (1975).

22. H. SATO AND Y. HIROTSU, *Mater. Res. Bull.* **11,** 1307 (1976).
23. D. J. M. BEVAN, B. HUDSON, AND P. T. MOSELEY, *Mater. Res. Bull.* **9,** 679 (1974).
24. M. HARATA, *Mater. Res. Bull.* **6,** 461 (1971).
25. L. A. BURSILL, B. G. HYDE, O. TERASAKI, AND D. WATANABE, *Philos. Mag.* **20,** 347 (1969).
26. J. VAN LANDUYT AND S. AMELINCKX, *Mater. Res. Bull.* **5,** 267 (1970).
27. K. KOSUGE AND S. KACHI, *Chem. Scr.* **8,** 70 (1975).
28. L. A. BURSILL, *Proc. Roy. Soc. Ser. A* **311,** 267 (1969).
29. E. IGUCHI AND R. J. D. TILLEY, *J. Solid State Chem.* **21,** 49 (1977).
30. Y. SHIMIZU AND E. IGUCHI, *Phys. Rev. B* **17,** 2505 (1978).
31. S. ANDERSSON AND A. D. WADSLEY, *Nature (London)* **211,** 581 (1969).